J. At. Mol. Sci.
doi: 10.4208/jams.062512.073012a

Vol. **4** , No. 3 , pp. 210-224
August 2013

A computational perspective of the competitive decomposition and isomerization of CH_3OCHFO radical

Hari Ji Singh*and Bhupesh Kumar Mishra

Department of Chemistry, DDU Gorakhpur University, Gorakhpur - 273009, India

Received 25 June 2012; Accepted (in revised version) 30 July 2012
Published Online 28 June 2013

Abstract. A detailed quantum chemical study is performed on the mechanism of the CH_3OCHFO radical formed during the photooxidation of CH_3OCH_2F (HFE-161), including the main decomposition and isomerization processes at the G2(MP2)//MPWB1K level of theory. The results clearly point out that the β -C-H bond scission is the dominant path involving the lowest energy barrier of 8.16 kcal mol^{-1} calculated at G2(MP2) level of theory. On the basis of the results obtained during the present investigation, the thermal rate constant for the different reaction channels involved during the isomerization and decomposition processes of CH_3OCHFO are evaluated at 298 K and 1 atm using Canonical Transition State Theory. The results are compared with the data available in the literature.

PACS: 31.15.A, 31.15.E, 82.20.Kh, 82.30.Lp, 82.33.Tb

Key words: theoretical study, hydrofluoroethers, G2 method, isomerization, canonical transition state theory

1 Introduction

Concern over the global environmental consequences of fully halogenated chlorofluorocarbons (CFCs) has created a need to determine the potential impact of other halogenated organic compounds on stratospheric ozone. The absence of a H-atom in the CFCs does not allow them to be oxidized or photolyzed in the troposphere. Thus, such compounds are transported into the stratosphere and their subsequent decomposition can lead to chlorine catalyzed ozone depletion [1-4]. Because of the critical role played by CFCs in stratospheric ozone depletion, continuous efforts are being made to find replacement compounds. Recently, attention has been paid to hydrofluoroethers (HFEs) to be used as

*Corresponding author. *Email address:* hjschem50@gmail.com (H. J. Singh)

third generation replacements to CFCs and may find a place in the industry to be used as cleaning agents of electronic equipments, heat transfer agents in refrigeration systems and as carrier fluids for lubricant deposition [5,6]. One of the principal advantages of the HFEs is their shorter atmospheric lifetimes in comparison to HFCs which in turn lead to lower GWP [7]. The absence of chlorine atoms in HFEs would lead us to believe that such compounds have little impact on stratospheric ozone and that they would possess a negligible Ozone Depleting Potential (ODP) [8]. Several theoretical and experimental studies performed with a few HFEs have shown that HFEs possess physical and thermochemical properties similar to that of CFCs, HCFCs and HFCs. Thus, the former can find acceptability in a wide variety of Industrial applications [9-13]. The low ozone depleting potential and shorter atmospheric life time (0.112 years) [14] of fluoromethyl methyl ether CH_3OCH_2F (HFE-161) and its comparable thermo-physical properties to CFCs regard it as the most suitable replacement for CFCs as a refrigerant. A general mechanism of tropospheric degradation of HFE-161 is shown in Fig. 1 which is based on the fact that initial attack of OH radical leads to the formation of haloalkyl radical ($CH_3OCHF^{\bullet}$). The latter reacts with atmospheric O_2 to produce peroxy radicals ($CH_3OCHFO_2^{\bullet}$). In a polluted atmosphere the peroxy radicals thus formed may further react with other oxidizing species such as NO_2 and NO that ultimately leads to the formation of haloalkoxy radical. On the other hand, haloalkoxy radical may also be generated through another intermediate, the hydroperoxide (CH_3OCHFO_2H) formed by the reaction of CH_3OCHFO_2 and HO_2. The haloalkoxy radicals thus formed play a critical role in removing a variety of organic vapours present in the troposphere [15]. Therefore, it is pertinent to perform experimental and theoretical studies on the decomposition of HFEs in order to ascertain their suitability as replacement compounds of CFCs.

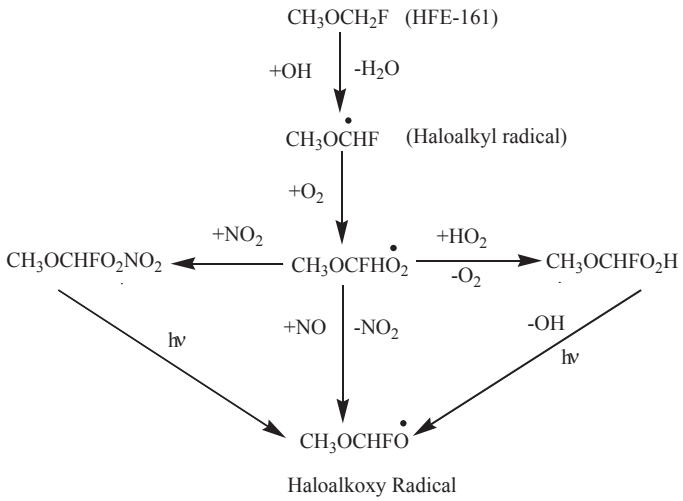

Figure 1: Tropospheric degradation mechanism of HFE-161.

To the best of our knowledge, no theoretical/experimental studies on the decomposition kinetics of the titled radical (CH_3OCHFO) have been performed. However, Kaliginedi *et al.* [16] have reported rate coefficients for the reaction of HFE-161 with OH using ab-initio/DFT methods. Christensen *et al.* [17] studied the degradation pathways of a similar hydrofluoroether, CF_3OCH_3 (HFE-143a) using smog chamber/FTIR technique and concluded that the haloalkoxy radical (CF_3OCH_2O) produced from HFE-143a degraded primarily by the reaction with O_2 in the atmosphere. In another study, Good *et al.* [18] also investigated the atmospheric oxidation mechanism of HFE-143a, HFE-134 (CHF_2OCHF_2) and HFE-125 (CHF_2OCF_3) using experimental and ab-initio methods and proposed that H-atom abstraction reaction caused by photochemically produced hydroxyl radicals was the dominant path for removing these compounds from the troposphere. Amongst the many, the one issue that has not been addressed is the fate of these HFEs in the atmosphere after being attacked by OH radical. It is the main issue in this work that has been explored by examining the atmospheric degradation mechanism of HFE-161 as one of the important classes of HFEs. Actuated by such a goal, we would like to present a detailed study using ab-initio and DFT methods of the decomposition and isomerization pathways of the haloalkoxy radical formed as result of OH attack on HFE-161.

There are four potential pathways of decomposition of CH_3OCHFO produced from HFE-161 that involve bond scission and isomerization processes. These are represented as follows:

$$CH_3OCHFO \longrightarrow CH_3O + C(O)HF \quad (1)$$

$$\longrightarrow CH_3OCHO + F \quad (2)$$

$$\longrightarrow CH_3OC(O)F + H \quad (3)$$

$$\longrightarrow CH_2OCHFOH \quad (4)$$

The following issues are addressed in this work:

i. The overall reaction mechanism including bond scission and isomerization.

ii. The features of potential energy surface at the high level of theory including barrier height and heat of reactions.

iii. The thermal rate constants of various reaction channels.

In order to achieve the above mentioned goal energetic calculations are performed using the modified G2 method, the G2(MP2). Thermodynamic properties such as free energy of activation, reaction enthalpies and free energies have been calculated. Canonical Transition State Theory (CTST) is utilized to predict the rate constants for the above channels (1-4). Attempts have been made to search and characterize transition states on the corresponding potential energy surfaces and energy barriers to decomposition have also been determined. The Intrinsic Reaction Coordinate (IRC) calculation has been performed to confirm the smooth transition from reactant to products through the respective transition states.

2 Computational method

Ab-initio quantum mechanical calculations were performed with the Gaussian 09 suite of program [19]. Geometry optimization of the reactant, products and transition states were made at the MPWB1K level of theory [20] using 6-31+G(d,p) basis set. In particular, the hybrid meta density functional MPWB1K has been found to give excellent results for thermochemistry and kinetics and is known to produce reliable results [21]. In order to determine the nature of different stationary points on the potential energy surface, vibrational frequencies calculations were performed using the same level of theory at which the optimization was made. All the stationary points had been identified to correspond to stable minima by ascertaining that all the vibrational frequencies had real positive values. The transition states were characterized by the presence of only one imaginary frequency (NIMAG=1). To ascertain that the identified transition states connect reactant and products smoothly, intrinsic reaction coordinate (IRC) calculations [22] were performed at the MPWB1K/6-31+G(d,p) level. As the reaction energy barriers are very much sensitive to the theoretical levels, the higher-order correlation corrected relative energies along with the density functional energies are necessary to obtain theoretically consistent reaction energies. Therefore, a potentially high-level method such as G2(MP2) has been used for single-point energy calculations. The G2(MP2) [23] energy is calculated in the following manner:

$$E[\text{G2(MP2)}]=E_{base}+\Delta E(\text{MP2})+\text{HLC}+\text{ZPE}$$

where, E_{base}=E[QCISD(T)/6-311G(d,p)], ΔE(MP2)=E[MP2/6-311+G(3df,2p)]-E[MP2/6-311G(d,p)], and HLC (High Level Correction)=-0.00481n_β - 0.00019n_α (n_α and n_β are the number of α and β valence electrons with $n_\alpha \geq n_\beta$) and ZPE = Zero-point energy.

In this method the geometry and frequency calculations were performed at MPWB1K/6-31+G(d,p) level. The ZPE thus obtained was corrected with a scale factor of 0.9537 to partly eliminate the systematic errors [20]. This dual level calculation (G2(MP2)//MPWB1K) is known to produce reliable kinetic data.

Table 1: Thermochemical data for the decomposition and isomerization channels of CH_3OCHFO calculated at MPWB1K/6-31+G(d, p) level. The values are given in kcal mol^{-1}.

Reaction channels	$\Delta G^{\#}$	$\Delta_r G^\circ$	$\Delta_r H^\circ$	$\Delta_r E$
$CH_3OCHFO \longrightarrow CH_3O$+ C(O)HF	14.66	-9.30	2.85	2.00
$CH_3OCHFO \longrightarrow CH_3OC(O)H$+F	21.41	13.31	21.92	21.02
$CH_3OCHFO \longrightarrow CH_3OC(O)F$+H	13.19	-2.01	5.38	4.34
$CH_3OCHFO \longrightarrow CH_2OCHFOH$	15.59	-11.00	-10.58	10.85

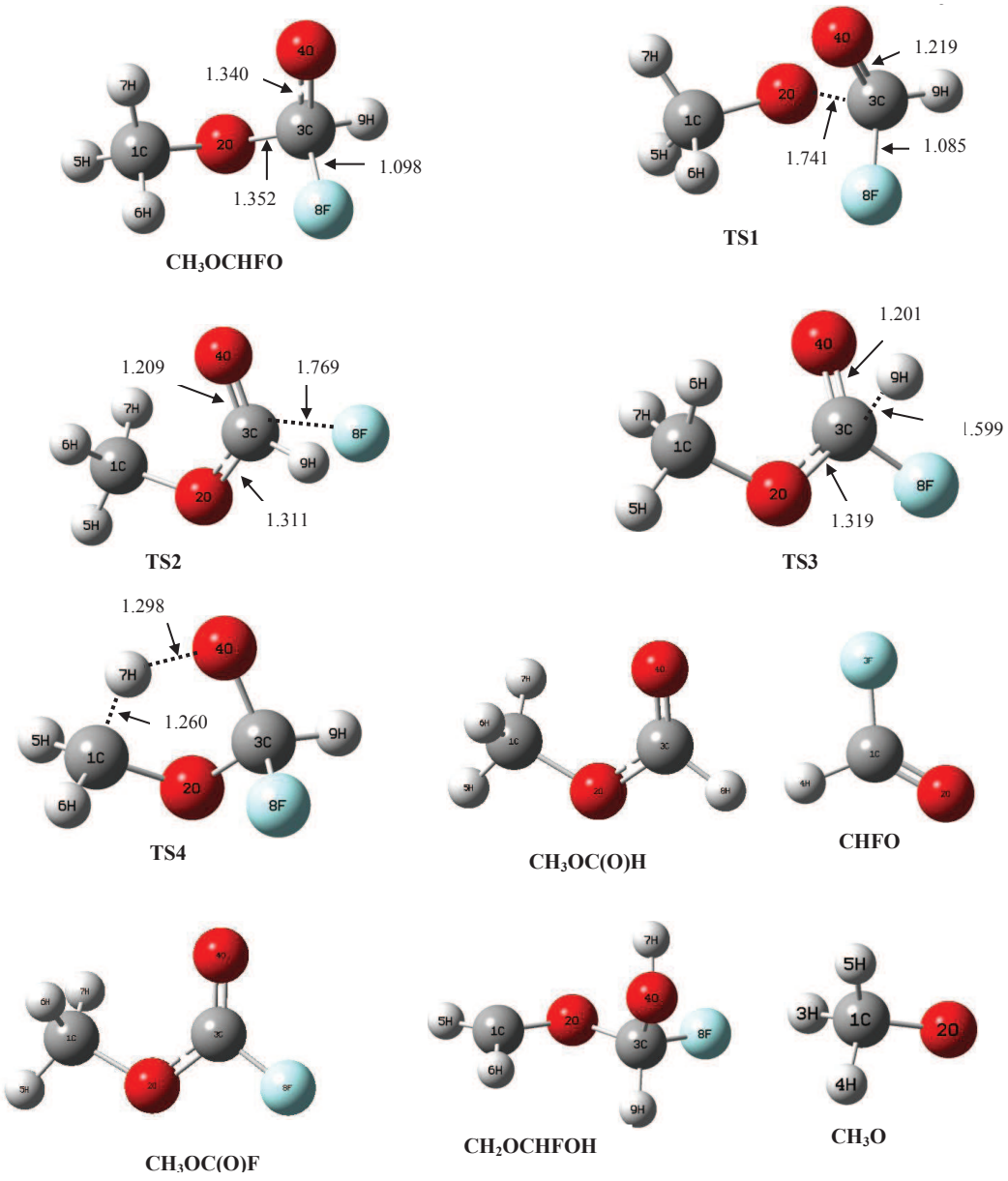

Figure 2: Optimized geometries of species involved in the decomposition and isomerization of CH_3OCHFO obtained at MPWB1K/6-31+G(d,p) level.

3 Results and discussion

The fate of haloalkoxy radical (CH_3OCHFO) during its thermal decomposition in the atmosphere is envisaged to occur via reactions (1-4). The detailed thermodynamic calcu-

lations performed at MPWB1K/6-31+G(d,p) level for free energies of activation, reaction enthalpies and free energies associated with reaction channels (1-4) are listed in Table 1. Results show that reaction (2) proceeds with an endothermicity of 21.92 kcal mol^{-1} along with a positive free energy change of 13.31 kcal mol^{-1}. This envisages that reaction (2) would be less probable. On the other hand, reactions 1, 3 and 4 proceed with negative free energies as listed in Table 1. Optimized geometries of reactant, products and transition states obtained at the MPWB1K/6-31+G(d,p) level are shown in Fig. 2. Transition states searched on the potential energy surfaces of reactions (1-4) are characterized as TS1, TS2, TS3 and TS4 respectively. The search was made along the minimum energy path on a relaxed potential energy surface. The geometrical parameters of the optimized structure of each species involved in reactions (1-4) are listed in the Supporting Information (Tables S1-S10). In the optimized structure of TS1 (Table S2) the elongation of the β -C-O bond (C3-O2) is found to be 1.352 to 1.741 Å (about 28% increases) with a simultaneous shrinkage of the C3-O4 bond. This decrease has been found to be almost 9% (1.340 to 1.219 Å). Similar analysis made on the optimized structure of TS2 (Table S3) reveals the elongation of C3-F8 bond length from 1.370 to 1.769 resulting in an increase of about 29% accompanied with a shrinkage of the β -C-O bond (C3-O2) 1.352 to 1.311 ($\sim$3%). The cleavage of the β -C-H bond (channel 3) leads to atomic hydrogen and $CH_3OC(O)F$ and

Table 2: Unscaled vibrational frequencies of reactant, products and transition states in CH_3OCHFO decomposition and isomerization at MPWB1K/6-31+G(d,p) level of theory.

Species	Vibrational frequencies (cm^{-1})
CH_3OCHFO	104, 197, 284, 502, 530, 726, 950, 1039, 1101, 1207, 1238, 1284, 1313, 1367, 1516, 1533, 1540, 3064, 3117, 3205, 3259
TS1	644i, 105, 149, 218, 357, 455, 676, 1018, 1116, 1145, 1169, 1211, 1398, 1444, 1474, 1535, 1638, 3086, 3171, 3183, 3201
TS2	396i, 149, 156, 297, 333, 443, 783, 997, 1026, 1208, 1232, 1362, 1405, 1489, 1524, 1529, 1616, 3155, 3247, 3253, 3283
TS3	1223i,143, 197, 307, 524, 567, 643, 710, 844, 1002, 1151, 1212, 1250, 1343, 1512, 1524, 1531, 1776, 3139, 3229, 3277
TS4	1985i, 143, 394, 511, 581, 630, 864, 1066, 1070, 1131, 1174, 1183, 1211, 1269, 1395, 1398, 1521, 1906, 3169, 3218, 3287
CH_3O	747, 993, 1176, 1412, 1413, 1550, 3019, 3101, 3144,
CHFO	686, 1070, 1154, 1410, 1989, 3212
$CH_3OC(O)H$	157, 314, 357, 803, 1007, 1080, 1209, 1227, 1319, 1433, 1507, 1523, 1530, 1895, 3144, 3174, 3233, 3272
$CH_3OC(O)F$	125, 192, 304, 594, 644, 801, 915, 1154, 1206, 1224, 1355, 1527, 1533, 1535, 2025, 3151, 3247, 3277
$CH_2OCHFOH$	88, 222, 300,370, 504, 509, 595, 655, 1024, 1147, 1203, 1256, 1326, 1356, 1411, 1463, 1519, 3192, 3253, 3393, 3938

Table 3: Calculated energy barriers in kcal mol^{-1}.

	G2(MP2)	MPWB1K
TS1	11.30	15.09
TS2	27.43	21.52
TS3	8.16	13.26
TS4	14.55	15.16

the corresponding transition state TS3 (Table S4) shows major structural changes than TS1 i.e., a substantial elongation ($\sim$46%) in the C3-H9 bond and a shortening ($\sim$2%) of the β -C-O bond (C3-O2).

The only possible rearrangement pathway through a five-membered ring type transition state TS4 leads to the formation of $CH_2OCHFOH$. The main structural characteristic of TS4 (Table S5) is the elongation of the C1-H7 bond by 15% and decrease of the O(2)C(1)H(7) angle from 110.4 Å in CH_3OCHFO to 96.2 Å in TS4 reflecting the migration of H(7) from C(1) to O(4).

Results obtained during frequency calculation for reactant, products and transition states involved in reactions (1-4) are recorded in Table. 2. These results show that the reactant and products have stable minima on their potential energy surface characterized by the occurrence of only real and positive vibrational frequencies. On the other hand, transition states are characterized by the occurrence of only one imaginary frequency obtained at 644, 396, 1223 and 1985 cm^{-1} for TS1, TS2, TS3 and TS4 respectively. Visualization of the listed imaginary frequencies using GaussView [24] gives a qualitative confirmation of the existence of transition states connecting reactant and products. The existence of a transition state on the potential energy surface, however, is ascertained by intrinsic reaction coordinate (IRC) calculation performed at the same level of theory using Gonzalez- Schlegel steepest descent path [22] in the mass weighted Cartesian coordinates with a step size of 0.05 ($amu^{1/2}$- bohr). Force constants at 31 selected points (15 in the reactant channel and 15 in the product channel) were calculated. The associated energy barriers corresponding to reactions (1-4) are recorded in Table. 3. No experimental or theoretical data are available in the literature to compare the energy barriers associated with the decomposition channels of CH_3OCHFO considered during the present investigation. However, to ascertain the reliability of the calculated values a comparison is made with the energy values calculated at B3LYP/6-311+G(2d,2p)//B3LYP/6-31G(d) by Good *et al.* [18] for structurally similar compounds CF_3OCF_2O (HFE-125) and CHF_2OCF_2O (HFE-134) yielding the energy barrier for β -C-O bond scission to be 9.4 and 10.30 kcal mol^{-1} respectively whereas corresponding values for the F-elimination process were found to be 22.8 and 25.8 kcal mol^{-1}. The results obtained during the course of the present investigation for β -C-O bond scission and F-elimination as 8.16 and 27.43 kcal mol^{-1} respectively for CH_3OCHFO radical decomposition show a good agreement with the data obtained by Good *et al.* [18]. This validates the use of the dual level calculation

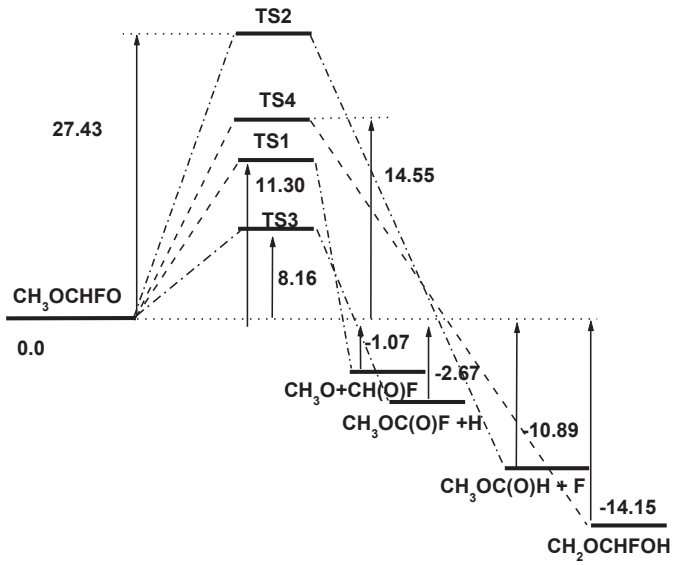

Figure 3: Energy level diagram for CH_3OCHFO unimolecular decomposition and isomerization at the G2(MP2) level. Energy values are given in kcal mol^{-1}.

of the species involved to construct a potential energy diagram for the decomposition channels of CH_3OCHFO. The zero-point corrected total energies are used relative to the ground state energy of CH_3OCHFO taken as zero and an energy diagram is constructed as shown in Fig. 3. The barrier height of 8.16 kcal mol^{-1} for β -C-H bond scission is considerably lower than that for other decomposition pathways and the dominance of the β -C-H bond scission in the decomposition of this haloalkoxy radical in the atmosphere is thus envisioned. Spin contamination was not important for the CH_3OCHFO radical because $<S^2>$ was 0.76 before annihilation which is only slightly larger than the expected value of $<S^2>$ = 0.75 for doublets.

4 Rate constants

The rate constants for the decomposition channels shown by reactions (1-4) of CH_3OCHFO radical are calculated using Canonical Transition State Theory (CTST) [25] using the following expression:

$$k = \Gamma(T)\frac{k_B T}{h}\frac{Q^{\ddagger}_{TS}}{Q_R}\exp\frac{-\Delta E}{RT} \tag{5}$$

where $\Gamma(T)$ is the tunneling correction factor at temperature T. $Q^{\ddagger}_{TS}$ and Q_R are the total partition functions for the transition state and reactant respectively. ΔE, k_B and h are the barrier height including ZPE, Boltzmann's and Planck's constants respectively. Calculation for the tunneling correction factor $\Gamma(T)$ was made using the expression of

Wigner [26] as given by the following expression:

$$\Gamma(T) = 1 + \frac{1}{24}\left(\frac{h\nu^{\#}}{k_B T}\right)^2 \tag{6}$$

where $\nu^{\#}$ is the imaginary frequency at the saddle point. However, the tunneling correction factor, (T) should be negligible for heavier atom/group as in the case of the reactions considered during the present study. The partition functions for the respective transition state and reactant at 298 K are obtained from the vibrational frequency calculation made at MPWB1K/6-31+G(d,p) level. Barrier heights were estimated from the energy difference including ZPE between TSs and reactant. The rate constant for β -C-O bond scission occurring via reaction (1) is calculated to be 5.85×10^{4} s^{-1} at 298 K and 1 atm. Based on a comparison with the decomposition of structurally similar haloalkoxy radicals CH_3OCH_2O for β -C-O bond scission, our calculated value comes out to be lower by an order of magnitude [27]. On the other hand, our modeling calculations performed for the A-factor for β -C-O bond scission comes out to be 1.10×10^{13} s^{-1} which is in good agreement with the value of $1-2\times10^{13}$ s^{-1} obtained by Good and Francisco [28]. The rate constant calculated for F-elimination and isomerization reactions are found to be 5.72×10^{-8} and 0.53×10^{2} s^{-1} respectively. Similar calculations performed to determine the rate constant for H-elimination occurring via reaction 3 involving TS3 as the transition state yielded a value of 5.15×10^{6} s^{-1} at 298 K and 1 atm with the associated A-factor of 4.91×10^{12} s^{-1}. We could not find any experimental data available in the literature to make a comparison with the calculated values obtained during the present investigation. Therefore, we performed kinetic calculations for a similar haloalkoxy radical, CH_2FCHFO for which experimental rate constant is available. Our calculation yielded a rate constant of 111×10^{4} s^{-1} for C-C bond scission whereas the detailed calculation performed by Hou *et al.* [29] resulted it to be 200×10^{4} s^{-1}. The experimental value for the same reaction has been reported to be 6×10^{4} s^{-1} in the lower limit by Wallington *et al.* [30]. We expect that the present study may provide useful information for future laboratory investigations.

5 Conclusions

We present here the potential energy profile (including geometries, energies and vibrational frequencies of reactant, transition states and products) and kinetic data for the thermal decomposition and isomerization of CH_3OCHFO radical investigated at the G2(MP2) //MPWB1K/6-31+G(d,p) level of theory. Energetic calculation reveals that the most dominant decomposition pathway for CH_3OCHFO is the β -C-H bond scission that occurs with a barrier height of 8.16 kcal mol^{-1}. The dominance of β -C-H bond scission in CH_3OCHFO is established during the present investigation which is in accord with the results obtained by Good and Francisco for structurally similar compound (oxygenated alkoxy radicals). The thermal rate constant evaluated using canonical transition state

theory for the dominant β -C-H scission channel is found to be 5.15×10^{6} s^{-1} with the corresponding A-factor as 4.91×10^{12} at 298 K and 1 atm pressure.

Acknowledgments This work is performed under the project sponsored by UP State Government under its Center of Excellence Program. The Research Associateship to BKM from CSIR, New Delhi is also acknowledged.

References

[1] J. D. Farman, B. G. Gardiner, and J. D. Shanklin, Nature 315 (1985) 207.
[2] M. J. Molina and F. S. Rowland, Nature 249 (1974) 810.
[3] F. S. Rowland and M. J. Molina, Chem. Eng. News 8 (1994) 72.
[4] D. J. Weubbles, J. Geophys. Res. 88 (1983) 1433.
[5] W. T. Tsai, J. Hazard. Mater. 119 (2005) 69.
[6] A. Sekiya and S. Misaki, J. Fluorine Chem. 101 (2000) 215.
[7] D. L. Cooper, T. P. Cunningham, N. L. Allan, and A. McCulloch, Atmos. Env. A 27 (1993) 117.
[8] R. A. Ravishankara, A. A. Turnipseed, N. R. Jensen, S. Barone, M. Mills, C. J. Howark, and S. Solomon, Science 263 (1994) 71.
[9] L. Chen, S. Kutsuna, K. Tokuhashi, and A. Sekiya, J. Phys. Chem. A 110(2006) 12845.
[10] S. Urata, A. Takada, T. Uchimaru, and A. K. Chandra, Chem. Phys. Lett. 368 (2003) 215.
[11] L. Chen, S. Kutsuna, K. Tokuhashi, A. Sekiya, K. Takeuchi, and T. Ibusuki, Int. J. Chem. Kinet. 35 (2003) 239.
[12] H. J. Singh and B. K. Mishra, J. Mol. Model. 16 (2010) 1473.
[13] H. J. Singh and B. K. Mishra, J. Mol. Model. 17 (2011) 415.
[14] P. Blowers, K. F. Tetrault, and Y. T. Morehead, Theor. Chem. Acc. 119 (2008) 369.
[15] T. J. Wallington, M. D. Hurley, J. M. Francheboud, J. J. Orlando, G. S. Tyndall, J. Sehested, T. E. Møgelberg, and O. J. Nielsen, J. Phys. Chem. 100 (1996)18116.
[16] K. Veerabhadrarao, M. A. Ali, and B. Rajakumar Int. J. Quan. Chem. 112 (2012) 1066.
[17] L. K. Christensen, T. J. Wallington, A. Guschin, and M. D. Hurly, J. Phys. Chem. A 102 (1999) 1854.
[18] D. A. Good, M. Kamboures, R. Santiano, and J. S. Francisco, J. Phys. Chem. 103 (1999) 9230.
[19] M. J. Frisch, G. W. Trucks, H. B. Schlegel, *et al.*, Gaussian 09, Rev. C 01 (Gaussian Inc., Pittsburgh PA, 2009).
[20] Y. Zhao and D. G. Truhlar, J. Phys. Chem. A 108 (2004) 6908.
[21] Y. Zhao, N. E. Schultz, and D. G. Truhlar, J. Chem. Theor. Comput. 2 (2006) 364.
[22] C. Gonzalez and H. B. Schlegel, J. Chem. Phys. 94 (1990) 5523.
[23] L. A. Curtiss, K. Raghavachari, and J. A. Pople J. Chem. Phys. 98 (1993) 1293.
[24] A. Frisch, A. B. Nielsen, and A. J. Holder, GaussView05 (Gaussian Inc., Wallingford CT, 2009).
[25] D. G. Truhlar, B. C. Garrett, and S. J. Klippenstein J. Phys. Chem. 100 (1996) 12771.
[26] E. P. Wigner, Z. Phys. Chem. B19 (1932) 203.
[27] E. Henon, F. Bohr, N. S. Gomex, and F. Caralp, Phys. Chem. Chem. Phys. 5 (2003) 5431.
[28] D. A. Good and J. S. Francisco, J. Phys. Chem. A 104 (2000) 1171.
[29] H. Hou, B. Wang, and Y. Gu, Phys. Chem. Chem. Phys. 2 (2000) 61.
[30] T. J. Wallington, M. D. Hurley, J. C. Ball, T. Ellermann, O. J. Nielsen, and J. Sehested, J. Phys. Chem. 98 (1994) 5435.

Appendix: Table S-I Optimized geometries of reactant in their ground state, transition states and products at MPWB1K/6-31+G(d,p) level of theory. [^{a}R (Bond length in Å); ^{b} (A) Angle in degree]

Table S1: Optimized geometrical parameters of CH_3OCHFO in the ground state.

Coordinates	MPWB1K/6-31+G(d,p)
R(1,2)^a	1.415
R(1,5)	1.082
R(1,6)	1.086
R(1,7)	1.088
R(2,3)	1.352
R(3,4)	1.340
R(3,8)	1.370
R(3,9)	1.098
A(2,1,5)^b	106.1
A(2,1,6)	110.7
A(2,1,7)	110.4
A(5,1,6)	109.7
A(5,1,7)	109.4
A(6,1,7)	110.1
A(1,2,3)	114.1
A(2,3,4)	115.8
A(2,3,8)	109.6
A(2,3,9)	108.5
A(4,3,8)	110.0
A(4,3,9)	104.0
A(8,3,9)	108.2

Table S2. Optimized geometrical parameters of TS1 in the ground state.

Coordinates	MPWB1K/6-31+G(d,p)
R(1,2)^a	1.391
R(1,5)	1.092
R(1,6)	1.086
R(1,7)	1.08
R(2,3)	1.741
R(3,4)	1.219
R(3,8)	1.346
R(3,9)	1.085
A(2,1,5)^b	103.9
A(2,1,6)	111.9
A(2,1,7)	111.3
A(5,1,6)	109.4
A(5,1,7)	108.3
A(6,1,7)	111.4
A(1,2,3)	113.8
A(2,3,4)	95.7
A(2,3,8)	102.0
A(2,3,9)	97.4
A(4,3,8)	119.0
A(4,3,9)	125.2
A(8,3,9)	109.6

Table S3. Optimized geometrical parameters of TS2 in the ground state.

Coordinates	MPWB1K/6-31+G(d,p)
R(1,2)[a]	1.422
R(1,5)	1.081
R(1,6)	1.084
R(1,7)	1.086
R(2,3)	1.311
R(3,4)	1.209
R(3,8)	1.769
R(3,9)	1.130
A(2,1,5)[b]	105.5
A(2,1,6)	110.3
A(2,1,7)	109.8
A(5,1,6)	110.6
A(5,1,7)	110.5
A(6,1,7)	109.7
A(1,2,3)	115.0
A(2,3,4)	126.8
A(2,3,8)	102.9
A(2,3,9)	112.8
A(4,3,8)	113.5
A(4,3,9)	116.7
A(8,3,9)	65.9

Table S4. Optimized geometrical parameters of TS3 in the ground state.

Coordinates	MPWB1K/6-31+G(d,p)
R(1,2)[a]	1.419
R(1,5)	1.081
R(1,6)	1.086
R(1,7)	1.084
R(2,3)	1.319
R(3,4)	1.201
R(3,8)	1.349
R(3,9)	1.599
A(2,1,5)[b]	105.2
A(2,1,6)	110.4
A(2,1,7)	110.7
A(5,1,6)	109.9
A(5,1,7)	110.3
A(6,1,7)	109.9
A(1,2,3)	118.8
A(2,3,4)	124.4
A(2,3,8)	111.2
A(2,3,9)	100.7
A(4,3,8)	121.03
A(4,3,9)	92.3
A(8,3,9)	94.9

Table S5. Optimized geometrical parameters of TS4 in the ground state.

Coordinates	MPWB1K/6-31+G(d,p)
R(1,2)a	1.386
R(1,5)	1.081
R(1,6)	1.08
R(1,7)	1.260
R(2,3)	1.371
R(3,4)	2.206
R(3,8)	1.356
R(3,9)	1.372
A(2,1,5)b	1.085
A(2,1,6)	1.298
A(2,1,7)	112.3
A(5,1,6)	114.7
A(5,1,7)	96.2
A(6,1,7)	115.6
A(1,2,3)	110.4
A(2,3,4)	105.3
A(2,3,8)	104.6
A(2,3,9)	74.7
A(4,3,8)	108.5
A(4,3,9)	111.3
A(8,3,9)	110.0

Table S6. Optimized geometrical parameters of CH_3O in the ground state.

Coordinates	MPWB1K/6-31+G(d,p)
R(1,2)	1.358
R(1,3)	1.099
R(1,4)	1.092
R(1,5)	1.092
A(2,1,3)	105.1
A(2,1,4)	112.8
A(2,1,5)	112.9
A(3,1,4)	106.8
A(3,1,5)	106.9
A(4,1,5)	111.5

Table S7. Optimized geometrical parameters of C(O)HF in the ground state.

Coordinates	MPWB1K/6-31+G(d,p)
R(1,2)	1.173
R(1,3)	1.329
R(1,4)	1.088
A(2,1,3)	122.6
A(2,1,4)	127.6
A(3,1,4)	109.6

Table S8. Optimized geometrical parameters of CH_3OCHO in the ground state.

Coordinates	MPWB1K/6-31+G(d,p)
R(1,2)	1.419
R(1,5)	1.081
R(1,6)	1.085
R(1,7)	1.085
R(2,3)	1.321
R(3,4)	1.195
R(3,8)	1.091
A(2,1,5)	105.8
A(2,1,6)	110.2
A(2,1,7)	110.2
A(5,1,6)	110.6
A(5,1,7)	110.6
A(6,1,7)	109.0
A(1,2,3)	115.3
A(2,3,4)	125.2
A(2,3,8)	109.9
A(4,3,8)	124.7

Table S9. Optimized geometrical parameters of CH_3OCFO in the ground state.

Coordinates	MPWB1K/6-31+G(d,p)
R(1,2)	1.423
R(1,5)	1.081
R(1,6)	1.084
R(1,7)	1.084
R(2,3)	1.306
R(3,4)	1.176
R(3,8)	1.337
A(2,1,5)	105.0
A(2,1,6)	110.5
A(2,1,7)	110.5
A(5,1,6)	110.2
A(5,1,7)	110.2
A(6,1,7)	110.0
A(1,2,3)	120.0
A(2,3,4)	126.4
A(2,3,8)	111.4
A(4,3,8)	122.0

Table S10. Optimized geometrical parameters of $CH_2OCHFOH$ in the ground state.

Coordinates	MPWB1K/6-31+G(d,p)
R(1,2)	1.352
R(1,5)	1.073
R(1,6)	1.078
R(2,3)	1.380
R(3,4)	1.351
R(3,8)	1.352
R(3,9)	1.087
R(4,7)	0.959
A(2,1,5)	113.5
A(2,1,6)	118.3
A(5,1,6)	122.8
A(1,2,3)	115.4
A(2,3,4)	113.1
A(2,3,8)	104.2
A(2,3,9)	111.7
A(4,3,8)	110.8
A(4,3,9)	107.9
A(8,3,9)	108.8
A(3,4,7)	108.9